Available online at www.sciencedirect.com
ScienceDirect
Journal of Sound and Vibration 323 (2009) 555–573
JOURNAL OF SOUND AND VIBRATION
www.elsevier.com/locate/jsvi

Feedforward control of bending waves in frequency domain at structural junctions using an impedance formulation

Jonas L. Svensson[a,*], Patrik B.U. Andersson[a], Joachim Scheuren[b,1], Wolfgang Kropp[a]

[a]*Division of Applied Acoustics, Chalmers University of Technology, 41296 Göteborg, Sweden*
[b]*Müller-BBM GmbH, 82152 Planegg, Germany*

Received 21 May 2008; received in revised form 13 January 2009; accepted 14 January 2009
Handling Editor: C.L. Morfey
Available online 20 February 2009

Abstract

This paper presents an active impedance-matching technique for vibrating structures described by Euler–Bernoulli theory. Full 2×2 impedance matrices are included in the derivation of the reflection matrix of an arbitrary structural junction. This implies that the effects of both bending waves and bending near-fields are included. An active impedance load is introduced in order to match a discontinuity at the junction, i.e. to force the reflection matrix to zero. The impedance-matching technique is applied to two theoretical examples. First, maximum power transfer at a free end is investigated under the condition of incident bending wave and bending near-field; second, the approach is used to match the junction between an Euler–Bernoulli beam and a sandwich composite for an incident bending wave. The latter example proposes an active–passive damping configuration which employs active control to enclose all incident wave power in a dissipative sandwich-type structure. Results show that for this configuration, the active impedance load is responsible for the main part of the power absorption over a broad frequency range.

1. Introduction

Impedance matching has shown potential to reduce low-frequency vibrations, e.g. [1]. Impedance matching is a concept that originates from the field of electrical networks, e.g. [2], and has a broad range of applications such as electrical noise cancellation in cellular phones [3] and as microwave amplifiers [4]. The fundamental principle is to match the characteristic impedance of a circuit to that of a load, thereby achieving maximum power transfer from circuit to load. The theory of circuit analogy [5] has rendered the application of impedance matching relatively straightforward in mechanical and acoustical systems, e.g. [6,7].

*Corresponding author. Tel.: +46 31 772 2209; fax: +46 31 772 2212.
E-mail address: jonas.svensson@chalmers.se (J.L. Svensson).
[1]This work was carried out under the author's adjunct professorship at the division of Applied Acoustics at Chalmers University of Technology.

0022-460X/$ - see front matter © 2009 Elsevier Ltd. All rights reserved.
doi:10.1016/j.jsv.2009.01.024

For acoustical systems, impedance matching has been used in hybrid passive–active acoustic absorbers. Beyene et al. [8] placed a loudspeaker behind a passive absorber at the boundary of a duct. The loudspeaker was driven so that its impedance would mimic the characteristic impedance of air in order to maximise the absorption of incident wave power [9,10]. Impedance-matching techniques have also been used to minimise the power flowing from structural-acoustic boundaries [11].

In the field of sound propagation and electrical networks, impedance matching is based on a scalar impedance quantity relating the two field variables (voltage and current in electrical circuits, and pressure and velocity for sound propagation) of a second-order wave equation. Impedance matching in such systems has been studied extensively in the past. However, impedance matching for more complex systems, described by higher-order differential equations, has been studied less. An example is a beam-like structure in bending which can be described by the fourth-order Euler–Bernoulli bending-wave equation. The solution to this equation contains four field variables, which implies that a 2×2 impedance matrix is necessary to relate all the field variables. This makes the impedance matching more difficult to apply. Attempts have been made to adopt impedance matching to vibration control of structures in bending [1,12,13]. However, these studies only consider scalar impedances allowing a relatively straightforward analogy with electrical networks.

While research concerning impedance matching in acoustic absorbers has investigated the possibilities of passive–active damping [8–10], studies of impedance matching for vibrating structures have mainly considered only active control [1,12,13]. Studies of hybrid passive–active damping configurations for vibrating structures have instead mostly focused on active constrained layers (ACL), e.g. [14,15]. The main purpose of ACL is to use active control in order to increase the shearing losses in a passive viscoelastic layer. However, some aspects of ACL indicate that it may not be the optimal configuration combining active and passive damping. It is pointed out in [16] that the characteristics of the constraining layer are not optimal for the open loop performance of the ACL. Lam et al. [17] reported that the actuator action is reduced, compared to pure active control, because the actuator must act through the viscoelastic material. Several studies have focused on improving the efficiency of ACL and other hybrid passive–active damping treatments [17–20], but the question of which configuration is the most effective is still not answered.

This paper presents an approach to impedance matching for a beam structure described by the Euler–Bernoulli bending-wave equation and its application to passive–active damping. The reflection matrix at a beam junction is expressed as a function of four impedance matrices. Two of these describe the Euler–Bernoulli beam, a third represents an arbitrary junction, and the fourth is an external, active impedance load. The active impedance load is chosen in order to compensate for the impedance mismatch which may occur at the junction. In order to facilitate understanding of the technique, the junction is initially exemplified by a free end. As a second step, the free end is replaced by a sandwich composite completing the passive–active damping configuration. The purpose of the latter configuration is to use active control to force all incoming wave power into the sandwich composite which has high internal damping.

2. Euler–Bernoulli beam model

The impedance matching presented in this paper is based on the Euler–Bernoulli theory, which is used to describe the bending motion of beam structures. The Euler–Bernoulli theory neglects rotational inertia and shear deformation (i.e. infinite shear stiffness), and is therefore suitable to describe low-frequency vibration. The governing equation is given by

$$EI\frac{\partial^4}{\partial x^4}\xi + \rho S\frac{\partial^2}{\partial t^2}\xi = 0, \tag{1}$$

where ξ represents normal displacement, ρS the mass per unit length and EI the bending stiffness, and x and t the length and time coordinate, respectively. If the system undergoes harmonic motion, it can be assumed that a solution to the differential equation will have the form of a wave,

$$\tilde{\xi}(x,t) = \hat{\xi}e^{\tilde{k}x}e^{j\omega t}, \tag{2}$$

where $\tilde{k}$ is the wavenumber, ω is the angular frequency, x is the length coordinate of the beam, t is the time, j is the imaginary unit and $\hat{\xi}$ is the amplitude of the wave. Inserting the expression for $\tilde{\xi}$ (Eq. (2)) into Eq. (1) yields

the dispersion relation,

$$\tilde{k}^4 = \frac{\rho S}{EI}\omega^2. \tag{3}$$

From Eq. (3) four complex roots are obtained,

$$\tilde{k}_{\mathrm{I}} = -\mathrm{j}k, \quad \tilde{k}_{\mathrm{II}} = \mathrm{j}k, \quad \tilde{k}_{\mathrm{III}} = -k, \quad \tilde{k}_{\mathrm{IV}} = k, \tag{4a–d}$$

where k represents the bending wavenumber,

$$k = \sqrt{\omega}\sqrt[4]{\frac{\rho S}{EI}}. \tag{5}$$

Inserting these roots, Eqs. (4a)–4(d), into the wave approach (Eq. (2)) yields four different terms. Two of these terms represent propagating bending waves, while two are exponentially decaying terms, representing evanescent waves or bending near-fields. For simplicity, the bending waves and bending near-fields will henceforth be referred to as waves and near-fields.

The superposition of the waves and near-fields yields the normal displacement of the beam. For further derivations, it is advantageous to consider instead the normal velocity of the beam. For harmonic vibrations the velocity is obtained by multiplying the displacement by $\mathrm{j}\omega$. The Euler–Bernoulli beam contains four field quantities: normal velocity, v; rotational velocity, w; bending moment, M; and shear force, F. These field variables, with the sign convention given by Fig. 1, are related through

$$w = \frac{\partial v}{\partial x}, \quad M = \frac{-EI}{\mathrm{j}\omega}\frac{\partial w}{\partial x}, \quad F = -\frac{\partial M}{\partial x}. \tag{6a–c}$$

3. Characteristic impedance matrices

The characteristic impedance matrices of an Euler–Bernoulli beam can be derived for leftward and rightward travelling wave and near-field, respectively. The impedance matrix for the rightward travelling wave and near-field will be derived below and the matrix for leftward travelling wave and near-field is given by analogy. Consider a beam with a wave and a near-field propagating and decaying in the positive x-direction. The normal velocity field on the beam is given by

$$v(x) = a_p^+ \mathrm{e}^{-\mathrm{j}kx} + a_N^+ \mathrm{e}^{-kx}, \tag{7}$$

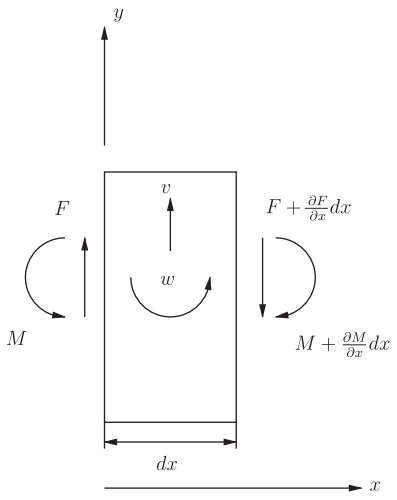

Fig. 1. A beam-element of length dx, v indicates lateral velocity, w rotational velocity, M bending moment and F shear force.

where a_p and a_N denote wave and near-field velocity amplitudes, respectively, and where the superscripts denote direction. For simplicity, the time dependence has been suppressed in Eq. (7). By inserting Eq. (7) into Eq. (6a)–(6c) the rotational velocity can be expressed as

$$w(x) = -\mathrm{j}ka_p^+ \mathrm{e}^{-\mathrm{j}kx} - ka_N^+ \mathrm{e}^{-kx}. \tag{8}$$

Eqs. (7) and (8) can be expressed in matrix form according to

$$\begin{Bmatrix} v(x) \\ w(x) \end{Bmatrix} = \begin{bmatrix} 1 & 1 \\ -\mathrm{j}k & -k \end{bmatrix} \begin{Bmatrix} a_p^+ \mathrm{e}^{-\mathrm{j}kx} \\ a_N^+ \mathrm{e}^{-kx} \end{Bmatrix}, \tag{9}$$

or more compactly as

$$\mathbf{u}(x) = \mathbf{C}^+ \boldsymbol{\Psi}^+(x)\mathbf{a}^+, \tag{10}$$

where

$$\mathbf{u}(x) = \begin{Bmatrix} v(x) \\ w(x) \end{Bmatrix}, \quad \mathbf{C}^+ = \begin{bmatrix} 1 & 1 \\ -\mathrm{j}k & -k \end{bmatrix},$$
$$\mathbf{a}^+ = \begin{Bmatrix} a_p^+ \\ a_N^+ \end{Bmatrix}, \quad \boldsymbol{\Psi}^+(x) = \begin{bmatrix} \mathrm{e}^{-\mathrm{j}kx} & 0 \\ 0 & \mathrm{e}^{-kx} \end{bmatrix}.$$

Multiplying Eq. (9), from the left, with the inverse of the matrix in the same equation gives

$$\begin{Bmatrix} a_p^+ \mathrm{e}^{-\mathrm{j}kx} \\ a_N^+ \mathrm{e}^{-kx} \end{Bmatrix} = \frac{1}{2} \begin{bmatrix} 1+\mathrm{j} & \frac{1+\mathrm{j}}{k} \\ 1-\mathrm{j} & \frac{-(1+\mathrm{j})}{k} \end{bmatrix} \begin{Bmatrix} v(x) \\ w(x) \end{Bmatrix}, \tag{11}$$

or

$$(\mathbf{C}^+)^{-1}\mathbf{u}(x) = \boldsymbol{\Psi}^+(x)\mathbf{a}^+. \tag{12}$$

Using relations (6a)–(6c) and (7), shear force and bending moment can be expressed as

$$\begin{Bmatrix} F(x) \\ M(x) \end{Bmatrix} = \frac{EIk^2}{\mathrm{j}\omega} \begin{bmatrix} \mathrm{j}k & -k \\ 1 & -1 \end{bmatrix} \begin{Bmatrix} a_p^+ \mathrm{e}^{-\mathrm{j}kx} \\ a_N^+ \mathrm{e}^{-kx} \end{Bmatrix}, \tag{13}$$

or more compactly as

$$\mathbf{Q}(x) = \mathbf{D}^+ \boldsymbol{\Psi}^+(x)\mathbf{a}^+, \tag{14}$$

where

$$\mathbf{Q}(x) = \begin{Bmatrix} F(x) \\ M(x) \end{Bmatrix}, \quad \mathbf{D}^+ = \frac{EIk^2}{\mathrm{j}\omega} \begin{bmatrix} \mathrm{j}k & -k \\ 1 & -1 \end{bmatrix}.$$

The right-hand side of Eq. (11) can be inserted into Eq. (13), which yields

$$\begin{Bmatrix} F(x) \\ M(x) \end{Bmatrix} = \frac{EI}{\omega} \begin{bmatrix} (1+\mathrm{j})k^3 & k^2 \\ k^2 & (1-\mathrm{j})k \end{bmatrix} \begin{Bmatrix} v(x) \\ w(x) \end{Bmatrix}. \tag{15}$$

This matrix can be recognised as the characteristic impedance matrix for an Euler–Bernoulli beam with a wave and a near-field propagating, respectively, decaying in the positive x-direction. This matrix has previously been derived in Ref. [21]. Here it is derived again for completeness sake and to introduce matrix variables. Eq. (15) can be expressed in matrix form: inserting Eq. (12) into Eq. (14) yields

$$\mathbf{Q}(x) = \mathbf{D}^+(\mathbf{C}^+)^{-1}\mathbf{u}(x), \tag{16}$$

and thus

$$\tilde{\mathbf{Z}}^{+} = \mathbf{D}^{+}(\mathbf{C}^{+})^{-1}. \tag{17}$$

A similar characteristic impedance matrix for wave and near-field in the negative x-direction can be expressed as

$$\tilde{\mathbf{Z}}^{-} = \mathbf{D}^{-}(\mathbf{C}^{-})^{-1}, \tag{18}$$

where

$$\mathbf{C}^{-} = \begin{bmatrix} 1 & 1 \\ \mathrm{j}k & k \end{bmatrix}, \quad \mathbf{D}^{-} = \frac{EIk^2}{\mathrm{j}\omega} \begin{bmatrix} -\mathrm{j}k & k \\ 1 & -1 \end{bmatrix},$$

and thus

$$\tilde{\mathbf{Z}}^{-} = \frac{EI}{\omega} \begin{bmatrix} -(1+\mathrm{j})k^3 & k^2 \\ k^2 & (\mathrm{j}-1)k \end{bmatrix}. \tag{19}$$

These impedance matrices are denoted by a tilde ($\tilde{\cdot}$) in order to separate them from the junction impedance matrix, which is introduced later. The difference between the wave impedance matrices for the positively and negatively propagating and decaying waves and near-fields (Eqs. (15) and (19)) is not an artefact of the beam properties, but merely the sign convention when the impedance matrices are defined. It is necessary to work with two different characteristic impedance matrices in order to set up the equilibrium conditions at a beam junction.

4. Beam junction impedance matrix

A beam junction is, in this paper, defined as any point, x_j, on the beam where the beam properties change abruptly. At this point any incident wave field can be scattered. The junction might represent a connection between two beams with different properties, the point where an external force or moment is introduced, or even a beam termination. At the beam termination, boundary conditions may be specified on two of the field variables: e.g. a free end is achieved by setting the bending moment and shear force to zero at the junction. By employing an impedance condition relating all four field variables, the junction can be kept arbitrary; see Fig. 2. The impedance condition is represented by a 2×2 matrix, here referred to as a junction-impedance matrix. The junction-impedance matrix relates the field variables according to

$$\begin{Bmatrix} F(x_0) \\ M(x_0) \end{Bmatrix} = \hat{\mathbf{Z}} \begin{Bmatrix} v(x_0) \\ w(x_0) \end{Bmatrix}, \tag{20}$$

where $\hat{\mathbf{Z}}$ is the junction-impedance matrix and x_0 is the co-ordinate at the junction. Any wave field entering this junction will be reflected according to a reflection matrix. This matrix describes the relation between incident and reflected waves and near-fields according to

$$\mathbf{a}^{-} = \mathbf{r}\mathbf{a}^{+}, \tag{21}$$

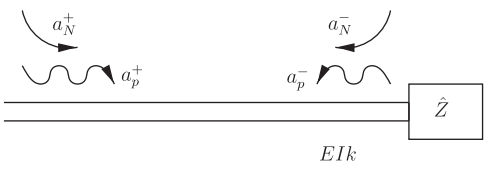

Fig. 2. The waves present on a waveguide terminated by an arbitrary junction impedance.

where $\mathbf{r}$ is the reflection matrix and $\mathbf{a}^-$ is defined as

$$\mathbf{a}^- = \begin{Bmatrix} a_p^- \\ a_N^- \end{Bmatrix}. \tag{22}$$

This vector contains the velocity amplitudes of a wave and a near-field in the negative x-direction. Furthermore, by defining a propagation matrix for this wave and near-field according to

$$\mathbf{\Psi}^-(x) = \begin{bmatrix} \mathrm{e}^{\mathrm{j}kx} & 0 \\ 0 & \mathrm{e}^{kx} \end{bmatrix}, \tag{23}$$

equilibrium at the beam junction can be stated as

$$\hat{\mathbf{Z}}\left(\begin{bmatrix} 1 & 1 \\ -\mathrm{j}k & -k \end{bmatrix}\mathbf{\Psi}^+\mathbf{a}^+ + \begin{bmatrix} 1 & 1 \\ \mathrm{j}k & k \end{bmatrix}\mathbf{\Psi}^-\mathbf{a}^-\right) = \frac{k^2EI}{\mathrm{j}\omega}\begin{bmatrix} \mathrm{j}k & -k \\ 1 & -1 \end{bmatrix}\mathbf{\Psi}^+\mathbf{a}^+ + \frac{k^2EI}{\mathrm{j}\omega}\begin{bmatrix} -\mathrm{j}k & k \\ 1 & -1 \end{bmatrix}\mathbf{\Psi}^-\mathbf{a}^-. \tag{24}$$

Equilibrium can also be stated by using matrix notation according to

$$\hat{\mathbf{Z}}(\mathbf{C}^+\mathbf{\Psi}^+\mathbf{a}^+ + \mathbf{C}^-\mathbf{\Psi}^-\mathbf{a}^-) = \mathbf{D}^+\mathbf{\Psi}^+\mathbf{a}^+ + \mathbf{D}^-\mathbf{\Psi}^-\mathbf{a}^-. \tag{25}$$

Inserting Eq. (21) into Eq. (25) and rearranging yields

$$\mathbf{r} = (-\hat{\mathbf{Z}}\mathbf{C}^-\mathbf{\Psi}^- + \mathbf{D}^-\mathbf{\Psi}^-)^{-1}(\hat{\mathbf{Z}}\mathbf{C}^+\mathbf{\Psi}^+ - \mathbf{D}^+\mathbf{\Psi}^+). \tag{26}$$

Finally, inserting Eqs. (17) and (18) into Eq. (26) yields

$$\mathbf{r} = (\mathbf{C}^-\mathbf{\Psi}^-)^{-1}(\tilde{\mathbf{Z}}^- - \hat{\mathbf{Z}})^{-1}(\hat{\mathbf{Z}} - \tilde{\mathbf{Z}}^+)\mathbf{C}^+\mathbf{\Psi}^+. \tag{27}$$

Expressing the reflection matrix in this manner makes it evident how the difference between the beam's characteristic impedance and the junction impedance determines the reflection matrix. Eq. (27) shows a clear analogy with the longitudinal wave case. In fact, if the matrices in Eq. (27) are replaced by their scalar equivalents, the reflection matrix is reduced to the well-known scalar reflection factor for longitudinal waves.

5. Deriving the scattering matrices for a connection of two Euler–Bernoulli beams

Eq. (27) yields the reflection matrix of an arbitrary beam junction. In this section the impedance approach will be used to derive the scattering matrices, i.e. reflection and transmission matrices, for a junction of two Euler–Bernoulli beams, where the receiving beam is semi-infinite. This is done to facilitate understanding of Eq. (27) and to illustrate the simplicity of using an impedance approach to derive the reflection matrix of structural junctions. The junction impedance is chosen as the characteristic impedance matrix representing a semi-infinite beam with a bending wavenumber and bending stiffness which are different from those of the first beam. A wave and a near-field are assumed to be incident, from the left beam, at the junction. The reflection matrix at $x_0 = 0$ becomes

$$\begin{aligned}\mathbf{r} &= (\mathbf{C}^-)^{-1}(\tilde{\mathbf{Z}}_1^- - \tilde{\mathbf{Z}}_2^+)^{-1}(\tilde{\mathbf{Z}}_2^+ - \tilde{\mathbf{Z}}_1^+)\mathbf{C}^+ \\ &= \frac{1}{\Delta}\begin{bmatrix} 2\alpha(1-\gamma^2) - \mathrm{j}\gamma(1-\alpha)^2 & \gamma(1+\mathrm{j})(1-\alpha^2) \\ \gamma(1-\mathrm{j})(1-\alpha^2) & 2\alpha(1-\gamma^2) + \mathrm{j}\gamma(1-\alpha)^2 \end{bmatrix},\end{aligned} \tag{28}$$

where

$$\Delta = 2\alpha(1+\gamma^2) + \gamma(1+\alpha)^2$$

and

$$\alpha = \frac{EI_2k_2^2}{EI_1k_1^2}, \quad \gamma = \frac{k_2}{k_1}.$$

Table 1
Some standard junction impedance matrices and the corresponding reflection matrix.

Case	$\hat{\mathbf{Z}}$	$\mathbf{r}$
Free end	$\mathbf{0}$	$\begin{bmatrix} -\mathrm{j} & 1+\mathrm{j} \\ 1-\mathrm{j} & \mathrm{j} \end{bmatrix}$
Continuous beam	$\tilde{\mathbf{Z}}^{+}$	$\mathbf{0}$
Point mass	$\begin{bmatrix} -\mathrm{j}\omega m & 0 \\ 0 & 0 \end{bmatrix}$	$\frac{1}{\Gamma}\begin{bmatrix} (1+\mathrm{j})k^3EI-2\omega^2 m & -2k^3EI \\ 2\mathrm{j}k^3EI & -(1+\mathrm{j})k^3EI-2\omega^2 m \end{bmatrix}$
Deflection spring	$\begin{bmatrix} \frac{\mathrm{j}K_d}{\omega} & 0 \\ 0 & 0 \end{bmatrix}$	$\frac{1}{\Omega}\begin{bmatrix} -\mathrm{j}(k^3EI+K_d-\mathrm{j}K_d) & (1+\mathrm{j})k^3EI \\ (1-\mathrm{j})k^3EI & \mathrm{j}(k^3EI-K_d+\mathrm{j}K_d) \end{bmatrix}$
Constants	$\Gamma = 2\omega^2 m - k^3EI(1-\mathrm{j})$	$\Omega = K_d + K_d\mathrm{j} + k^3EI$

The subscripts 1 and 2 given to the impedance matrices denote the beam to the left and right of the junction, respectively. A transmission matrix which relates incident wave and near-field to transmitted wave and near-field may also be calculated for this case:

$$\begin{aligned}\mathbf{t} &= \mathbf{C}_2^{+}(\mathbf{I}+(\tilde{\mathbf{Z}}_1^{-}-\tilde{\mathbf{Z}}_2^{+})^{-1}(\tilde{\mathbf{Z}}_2^{+}-\tilde{\mathbf{Z}}_1^{+}))\mathbf{C}^{+} \\ &= \frac{2}{\Delta}\begin{bmatrix} (1+\gamma)(\alpha-1) & (1-\mathrm{j}\gamma)(1-\alpha) \\ (1+\mathrm{j}\gamma)(\alpha-1) & (1+\gamma)(1+\alpha) \end{bmatrix},\end{aligned} \tag{29}$$

where $\mathbf{I}$ is a 2×2 unit matrix. The reflection and transmission matrices agree with those derived by stating continuity and equilibrium [22]. The given example illustrates the simplicity of deriving a reflection matrix for a beam junction by using this impedance formulation. Eq. (27) can be employed to calculate the reflection matrix for any type of junction on an Euler–Bernoulli beam. However, a requirement is that the junction impedance matrix can be calculated. Table 1 presents the impedance matrices and corresponding reflection matrices for some idealised junctions.

6. Active impedance load

The conventional approach to introduce active control at beam junctions in order to manipulate the junction reflection matrix is to introduce external forces or moments in the equilibrium conditions, e.g. Ref. [23]. When introducing external forces or moments for active control, the impedance formulation of the junction reflection matrix shows a substantial advantage compared to the more conventional formulation of stating continuity and equilibrium conditions. An active impedance load is introduced by simply splitting the junction impedance in Eq. (20) into a passive and an active part according to

$$\hat{\mathbf{Z}} = \hat{\mathbf{Z}}^{\mathrm{pass}} + \hat{\mathbf{Z}}^{\mathrm{act}}. \tag{30}$$

$\hat{\mathbf{Z}}^{\mathrm{pass}}$ represents an arbitrary passive system and $\hat{\mathbf{Z}}^{\mathrm{act}}$ an external, active impedance load, defined as

$$\hat{\mathbf{Z}}^{\mathrm{act}} = \begin{bmatrix} z_{11}^{\mathrm{act}} & z_{12}^{\mathrm{act}} \\ z_{21}^{\mathrm{act}} & z_{22}^{\mathrm{act}} \end{bmatrix}. \tag{31}$$

Each element of this matrix may be chosen arbitrarily and independently of the others. This matrix fundamentally works like a gain matrix that weights the lateral and rotational velocities at x_0 to give an actuation vector at this point according to

$$\mathbf{Q}^{\mathrm{act}}(x_0) = \mathbf{Z}^{\mathrm{act}}\mathbf{u}(x_0), \tag{32}$$

where

$$\mathbf{Q}^{\mathrm{act}} = \begin{Bmatrix} F^{\mathrm{act}} \\ M^{\mathrm{act}} \end{Bmatrix}, \quad \mathbf{u} = \begin{Bmatrix} v \\ w \end{Bmatrix}. \tag{33}$$

By obtaining the translational and rotational velocities at $x = x_0$, Eq. (32) can be used to derive the active force and moment that will modify the junction's reflective properties to adopt an arbitrary form. Thus the active impedance matrix couples two possible sensing modes (translational and rotational velocities) to two possible actuation modes (force and moment). Which of these modes are used depends on which of the elements in the active impedance matrix are non-zero. The ability to manipulate the reflection matrix at the junction means the ability of selective wave control. When introducing external forces or moments for active control, it is vital to have knowledge of how they affect the power flow in the system. The power injected by the active impedance load (force and moment) is given by

$$W_{\mathrm{in}}^{\mathrm{act}} = \tfrac{1}{2}\mathrm{Re}\{((\mathbf{C}^{+} + \mathbf{C}^{-}\mathbf{r})\mathbf{a}^{+})^{\mathrm{H}}\mathbf{Z}^{\mathrm{act}}(\mathbf{C}^{+} + \mathbf{C}^{-}\mathbf{r})\mathbf{a}^{+}\}, \tag{34}$$

where H denotes Hermitian transpose. When the sign of Eq. (34) is positive, power is injected to the beam, and when the sign is negative power, is absorbed. Thus, to drive an optimal active absorber the active impedance load can be chosen in a way which minimises Eq. (34).

7. Numerical examples

In order to demonstrate the performance of the impedance approach to active control, two numerical examples are presented in this section. First, the active impedance load is applied in order to absorb power at the free end of a beam; second, the active impedance load will be used to match the junction of an Euler–Bernoulli beam and a sandwich beam. The first example is given to illustrate the potential of using active impedance control at structural junctions and to facilitate understanding of the approach. The second example is given to explore the possibility of a passive–active damping configuration where the control objective is to confine all wave power to a passive absorber. The control laws are applied to the frequency domain models in order to see the impact on power transport and absorption as well as control effort.

7.1. Maximum power transfer

In this example the active impedance load will be applied with the passive junction impedance set to the null matrix so that $\hat{\mathbf{Z}} = \hat{\mathbf{Z}}^{\mathrm{act}}$. This is equivalent to active control at a free end. The objective is to choose $\hat{\mathbf{Z}}^{\mathrm{act}}$ in such a way that a maximum amount of power is transferred from the beam to the active impedance load, which in this case will work as an active absorber. The numerical values used for the implementation are given as base beam in Table 3. The beam is assumed to have no internal losses in order to simplify the power flow analysis. The upper frequency limit is set at 2000 Hz because active control is most advantageous at low frequencies. The bending wavelength at 2000 Hz for this beam is more than 10 times larger than any of the cross-sectional dimensions, and hence the assumptions of the Euler–Bernoulli theory can be considered to be valid.

An external point force somewhere on the beam will create a leftward propagating wave and decaying near-field, respectively, Fig. 3, with velocity amplitudes according to

$$\begin{Bmatrix} b_p^{+} \\ b_N^{+} \end{Bmatrix} = \frac{-\mathrm{j}\omega F^{\mathrm{p}}}{4EIk^3}\begin{Bmatrix} \mathrm{j} \\ 1 \end{Bmatrix}, \tag{35}$$

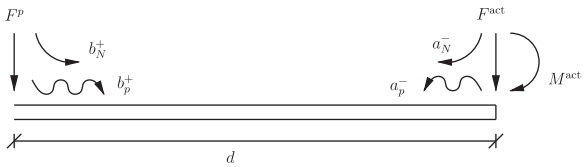

Fig. 3. The configuration investigated in the first numerical example.

where b is used to denote the amplitudes at the location of the force, and F^{p} represents the primary force. The amplitudes at the force location can be transformed to amplitudes at the junction using the propagation matrix $\mathbf{\Psi}^{+}$ according to

$$\begin{Bmatrix} a_p^+ \\ a_N^+ \end{Bmatrix} = \begin{bmatrix} \mathrm{e}^{-\mathrm{j}kd} & 0 \\ 0 & \mathrm{e}^{-kd} \end{bmatrix} \begin{Bmatrix} b_p^+ \\ b_N^+ \end{Bmatrix}, \tag{36}$$

where d is the distance between the primary force and the junction. In this paper it is assumed that the wave and near-field travelling to the left are not reflected at the primary force location. Thus, the incident wave field is completely determined by the primary force according to Eq. (35). This choice is motivated by the aim to study control of incident waves and near-fields at the junction. Thus, the aim is to test a wave controller and not necessarily a controller to work in a closed system.

7.1.1. Not considering an incident near-field

If d approaches infinity the incident near-field can be neglected (replacing the one with a zero in Eq. (35)) and only one actuation mode is necessary in order to absorb all the incident power. This has been shown theoretically by Ref. [1] and experimentally by Ref. [24]. Using only the $(1,1)$ element of the active impedance matrix, to cancel the $(1,1)$ element of the reflection matrix is equivalent to minimise Eq. (34), under the condition of only incident wave. The $(1,1)$ element of the active impedance matrix is chosen as the control variable while the other elements are set to zero. This is the most obvious choice since sensors to obtain normal velocity and actuators to apply force are common and have proven to work well. Inserting this matrix ($z_{11} \neq 0$, $z_{12} = z_{21} = z_{22} = 0$) as the junction matrix in Eq. (27) while requiring the $(1,1)$ element of the reflection matrix to be zero ($r_{11} = 0$) yields

$$r_{11} = 0 = \frac{\mathrm{j}(-z_{11}^{\mathrm{act}}\mathrm{j}\omega + z_{11}^{\mathrm{act}} + \omega k^3 EI)}{z_{11}^{\mathrm{act}}\omega - z_{11}^{\mathrm{act}}\mathrm{j}\omega + k^3 EI}. \tag{37}$$

In order for Eq. (37) to be fulfilled z_{11}^{act} has to be

$$z_{11}^{\mathrm{act}} = \frac{(1-\mathrm{j})}{2}\frac{k^3 EI}{\omega}, \tag{38}$$

which is half of the complex conjugate of the same element, $(1,1)$, in the characteristic impedance matrix, $\tilde{\mathbf{Z}}^{+}$, in Eq. (15). This agrees with the results previously reported in Ref. [1]. This control law will be referred to as maximum power-transfer control. If the active absorber would be placed in the middle of an infinite beam instead, the optimal active impedance load (z_{11}^{act}) that would minimise Eq. (34) would be twice the complex conjugate of the characteristic impedance ($\tilde{z}_{11}^{+}$). This would result in half the incident power being absorbed while one quarter is reflected and one quarter transmitted. The latter agrees with the results reported by Refs. [1,23].

By using the $(1,1)$ element, z_{11}^{act}, in the active impedance matrix, translational velocity is used as the sensing mode and force as the actuation mode. Although this choice would be the simplest to implement in reality, in theory any of the four elements in the active impedance matrix can be used. Using any of the two elements in the diagonal of the active impedance matrix, the control law is equal to half the complex conjugate of the corresponding element in the characteristic impedance matrix for positively travelling wave and near-field (Eq. (15)). Using either of the two elements in the skew diagonal of the active impedance matrix, the control law is equal to the corresponding element in the wave impedance matrix, for positively travelling wave and near-field, Eq. (15). These results are summarised in Table 2. The magnitude of the active force, using the $(1,1)$ element of the active impedance matrix, is plotted in Fig. 10. This result is normalised by the amplitude of the primary force.

7.1.2. Considering an incident near-field

For the case of controlling only an incident wave, all the net power is contained in the incident wave and all that power is absorbed by the active impedance load. This is trivial since there are no reflection, no interacting near-fields, no material losses in the beam and no power absorption by the passive junction impedance. Neglecting the incident near-field gives a scalar control law which agrees with previously reported results concerning power absorption of a free beam end. However, if the junction is located close to the primary

Table 2
The values of the elements of the active impedance matrix that will force r_{11} to zero.

Element	Control law
z_{11}	$\frac{\mathrm{conj}(\tilde{z}_{11}^{+})}{2}$
z_{12}	$\tilde{z}_{12}^{+}$
z_{21}	$\tilde{z}_{21}^{+}$
z_{22}	$\frac{\mathrm{conj}(\tilde{z}_{22}^{+})}{2}$

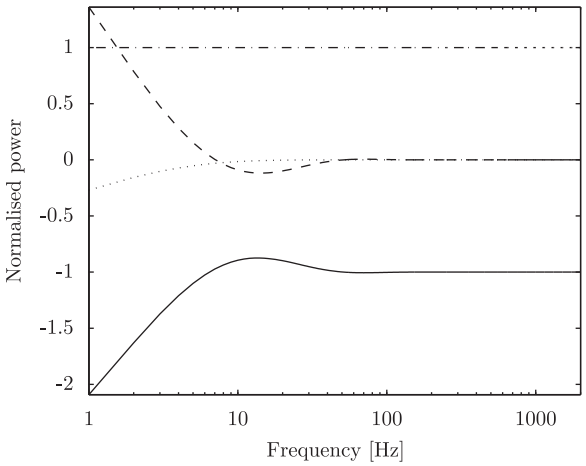

Fig. 4. The modes of power transport, for the maximum power transfer control, under the influence of an incident wave and a near-field. The primary force is located 1 m from the junction. —: power absorbed by the active impedance load; ...: power carried by the wave propagating in the negative direction; -.-: power carried by the incident wave; - - -: power propagated by the interacting near-fields. The results are normalised with the power carried by the wave propagating in the positive direction.

excitation it is important also to consider an incident near-field. The full reflection matrix, using the maximum power-transfer control law of Eq. (38), is

$$\mathbf{r}^{\mathrm{MPT}} = \begin{bmatrix} 0 & \mathrm{j} \\ 1 & \mathrm{j}-1 \end{bmatrix}. \tag{39}$$

The superscript MPT denotes maximum power transfer. The reflection matrix shows that any incident near-field will give rise to an equally large (in amplitude) but phase-shifted (90°) reflected propagating wave, element (1, 2) in Eq. (39). Thus in the presence of a significant near-field this controller would perform poorly, in terms of cancelling the reflected wave. There is leftward propagating power carried by the reflected wave. Hence, all the incident power is not absorbed but some is instead reflected. Figs. 4 and 5 present the power transport for two different distances between primary excitation to the junction, 1 and 0.1 m, respectively. The graphs in the figures represent the different modes of power transport, i.e. the power carried by the positively propagating wave, negatively propagating wave and interacting near-fields, respectively, as well as the power absorbed by the active impedance load (force in this case). A negative sign means that power flows away from the junction and a positive sign means that power flows towards the junction. Fig 4 shows that power is carried by a negatively propagating wave only under 100 Hz when the primary force is located 1 m from the junction, while Fig. 5 shows that if the primary force is located 0.1 m from the junction, power is carried by a negatively travelling wave up to 2000 Hz. Fig. 5 also shows that below about 100 Hz the near-fields are responsible for the major part of the net power flow. The primary force is given a unit amplitude and zero

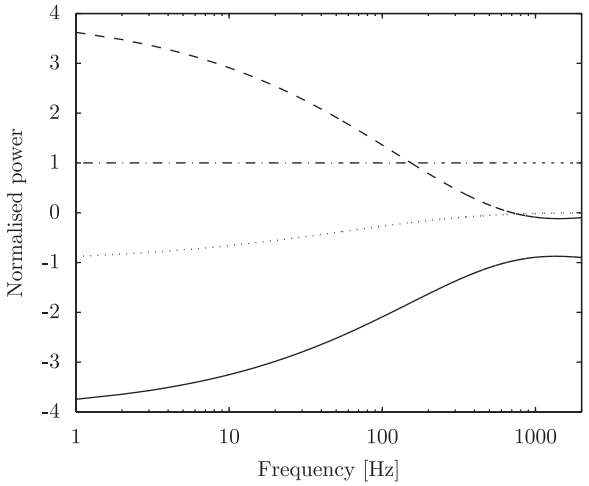

Fig. 5. The modes of power transport, for the maximum power transfer control, under the influence of an incident wave and a near-field. The primary force is located 0.1 m from the junction.—: power absorbed by the active impedance load; . . .: power carried by the wave propagating in the negative direction; - . -: power carried by the incident wave; - - -: power propagated by the interacting near-fields. The results are normalised with the power carried by the wave propagating in the positive direction.

Table 3
The numerical values used for the simulation of the impedance matching control law.

Material Unit	Thickness (mm)	Width (mm)	Density (kg/m^3)	E Modulus (MPa)	Loss fact. (-)	Poi. ratio (-)
Base beam	10	20	2700	69×10^3	0	–
VEM	0.1	20	1100	20	0.7	0.45
Cover layer	0.5	20	7800	61×10^3	0	

phase over the entire frequency range, 1–2000 Hz, and the material properties and geometry of the beam are given by Table 3 as base beam.

The reflection of a wave at the junction can be avoided even in the presence of both incident wave and near-field. By using two elements in the active impedance matrix, two elements in the reflection matrix can be set to zero. Hence, no propagating wave will be reflected at the boundary, not even in the presence of an incident near-field. This is achieved by choosing the active impedance matrix as

$$\mathbf{Z}^{\mathrm{act}} = \frac{EI}{\omega}\begin{bmatrix} k^3 & -\mathrm{j}k^2 \\ 0 & 0 \end{bmatrix}. \tag{40}$$

This still only requires one actuation mode, but two sensing modes. Inserting Eq. (40) into Eq. (27) yields the reflection matrix

$$\mathbf{r}^{\mathrm{noref}} = \begin{bmatrix} 0 & 0 \\ 1 & -1 \end{bmatrix}. \tag{41}$$

Figs. 6 and 7 show the power flow, when the active impedance matrix in Eq. (40) is used, for 0.1 and 1 m distance between the primary force and the junction, respectively. Cancellation of the reflected wave can also be achieved by using the diagonal elements in the active impedance matrix; however, this requires both two sensing modes and two actuation modes and is thus disadvantageous in comparison. To avoid reflection of both a wave and a near-field for an arbitrary incident wave field the reflection matrix must be the null matrix. This is achieved by setting the junction-impedance matrix equal to the characteristic impedance matrix of a

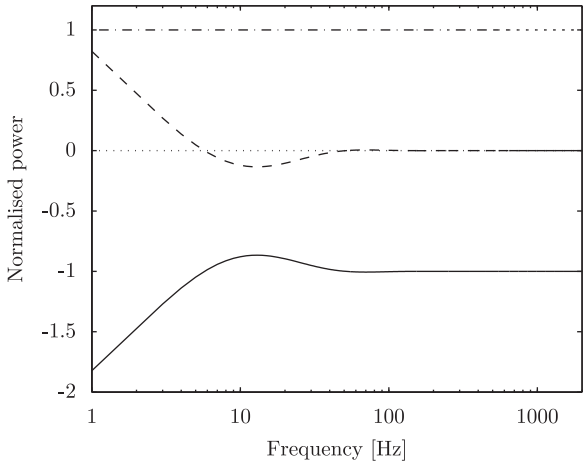

Fig. 6. The modes of power transport, for the control using two elements in the active impedance matrix, under the influence of an incident wave and a near-field. The primary force is located 1 m from the junction. —: power absorbed by the active impedance load; . . .: power carried by the wave propagating in the negative direction; - . -: power carried by the incident wave; - - -: power propagated by the interacting near-fields. The results are normalised with the power carried by the wave propagating in the positive direction.

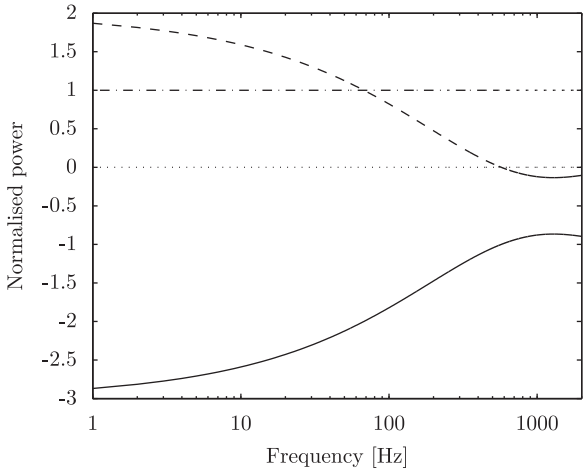

Fig. 7. The modes of power transport, for the control using two elements in the active impedance matrix, under the influence of an incident wave and a near-field. The primary force is located 0.1 m from the junction. —: power absorbed by the active impedance load; . . .: power carried by the wave propagating in the negative direction; - . -: power carried by the incident wave; - - -: power propagated by the interacting near-fields. The results are normalised with the power carried by the wave propagating in the positive direction.

positively travelling wave and near-field, thus extending the beam to infinity. This has previously been reported in Ref. [25].

7.2. *Active impedance matching between an Euler–Bernoulli beam and a sandwich composite*

The impedance approach will here be used in order to theoretically investigate the performance of a passive–active damping configuration. The characteristic impedance of a Euler–Bernoulli beam is matched to the impedance of a sandwich composite; see Fig. 8. The impedance approach proves very useful as it enables a lumped parameter description of a complex right-hand-side system. In some cases an analytical impedance matrix may be difficult to find. However, it is quite easy to calculate numerically on a computer. By applying a

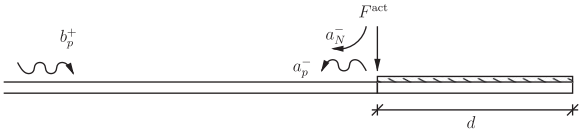

Fig. 8. The passive–active configuration using impedance-matching techniques, in the second numerical example.

force at the left boundary, two driving-point mobility functions can then be computed as

$$Y_{vF}(\omega) = \frac{v(\omega)}{F(\omega)}, \tag{42a}$$

$$Y_{wF}(\omega) = \frac{w(\omega)}{F(\omega)}. \tag{42b}$$

By applying a moment at the same boundary, two additional driving-point mobilities can be computed according to

$$Y_{vM}(\omega) = \frac{v(\omega)}{M(\omega)}, \tag{43a}$$

$$Y_{wM}(\omega) = \frac{w(\omega)}{M(\omega)}. \tag{43b}$$

These expressions (Eqs. (42a), (42b) and (43a), (43b)) can be organised in a matrix as

$$\mathbf{Y} = \begin{bmatrix} Y_{vF} & Y_{vM} \\ Y_{wF} & Y_{wM} \end{bmatrix}, \tag{44}$$

which is called a driving-point mobility matrix. This matrix can be inverted to give the driving-point impedance matrix according to

$$\mathbf{Z} = \mathbf{Y}^{-1}. \tag{45}$$

This impedance matrix can then be inserted as $\hat{\mathbf{Z}}^{\mathrm{pass}}$ into Eq. (27) to give the reflection matrix at the junction. Given any incident wave field it is then possible to obtain the total wave field on the Euler–Bernoulli beam.

By using a thin cover metal sheet to constrain a dissipative viscoelastic material placed on a base beam, the shear motion in the viscoelastic layer is increased and thereby also the losses. This type of sandwich structure is fairly common as a vibration damper, and is referred to as passive constrained layer damping (PCLD). The equations used here to describe the sandwich composite were derived in Ref. [26]. This model is based on Euler–Bernoulli theory for the base and cover beam, while only shear motion with a constant shear angle across the depth is assumed in the viscoelastic layer. The equations of motion and the solution to these are given in Appendix A.

The driving-point mobility matrix of a 0.35 m long, free–free sandwich composite with the properties given in Table 3, can be calculated (Eqs. (42a), (42b)–(44)) and inverted to give the driving-point impedance matrix according to Eq. (45). This impedance matrix can then be inserted into Eq. (27) to give the reflection matrix of a junction of an Euler–Bernoulli beam and a sandwich composite. The properties of the Euler–Bernoulli beam are given in Table 3 as base beam.

Only a propagating wave is incident at the junction. The total deflection field on the Euler–Bernoulli beam can be obtained by employing the numerically calculated reflection matrix. This approach gives exactly the same deflection field on the Euler–Bernoulli beam as if the beams had been connected in the standard way, through continuity and equilibrium conditions as in Ref. [27].

Fig. 9 shows the attenuation in the passive junction impedance (sandwich composite) for the case without control. The attenuation is given by the reflection efficiency, i.e. the absolute value squared of the $(1,1)$ element of the reflection matrix. By introducing an active impedance matrix any reflection from the junction can be avoided. Forcing the $(1,1)$ element of the reflection matrix to zero requires one sensing mode and one actuation mode. For this case the sensing mode is chosen as translational velocity and the actuation mode as

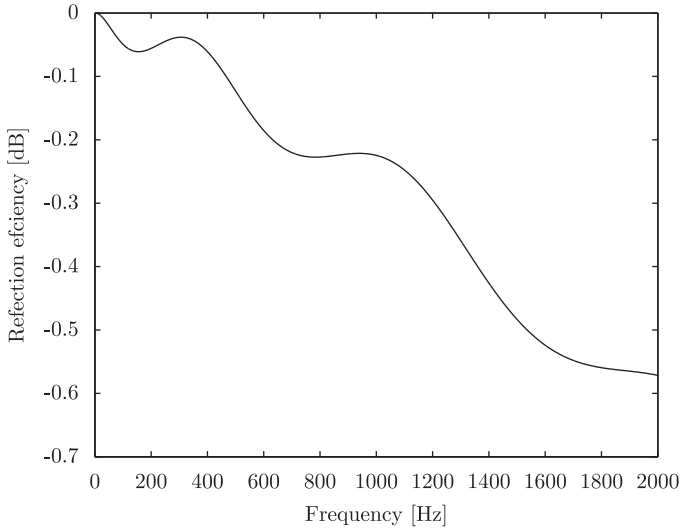

Fig. 9. The reflection efficiency at the junction of the Euler–Bernoulli and the sandwich composite, compared to the incident wave. For the case of no control at the junction.

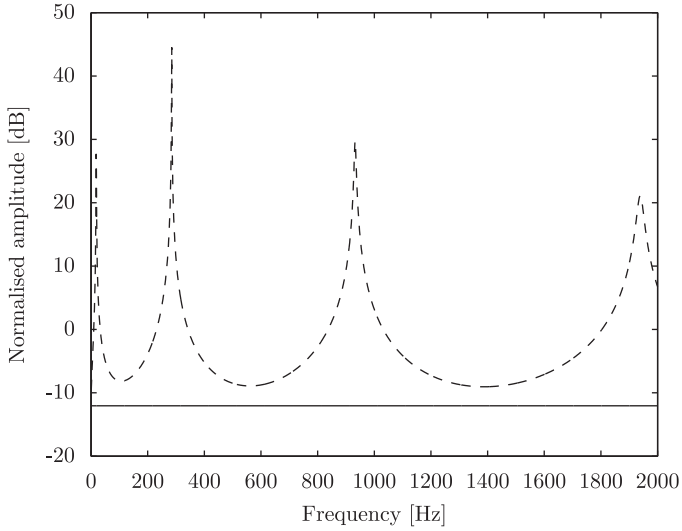

Fig. 10. The amplitude level of the active force. —: the maximum power transfer control law; - - -: the control law matching the impedance between the Euler–Bernoulli and sandwich composite.

force. The control effort is plotted in Fig. 10. The primary force is given a unit amplitude and zero phase over the entire frequency range, 1–2000 Hz.

Fig. 11 shows the amount of power which is either absorbed or injected by the active and passive junction impedances, respectively. The results are normalised by the power carried by the incident wave. Fig. 12 shows the sign of the power flow. A positive sign means that power is injected into the beam and a negative sign means that power is absorbed. These figures show that the active junction impedance is responsible for most of the power absorption over the entire investigated frequency range, except around resonances where the active impedance load injects power. The injected power in addition to the power carried by the incident wave is absorbed in the sandwich beam.

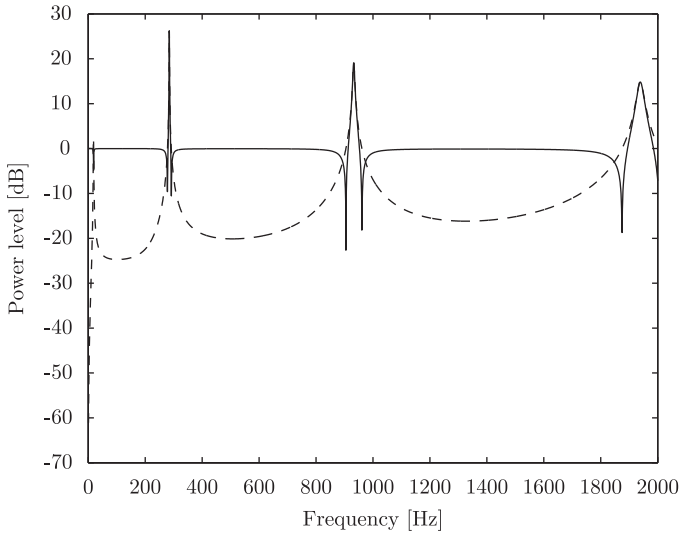

Fig. 11. The power injected or absorbed by the passive junction impedance (- - -) and the active impedance load (—), respectively. The results are normalised with the power carried by the incident wave.

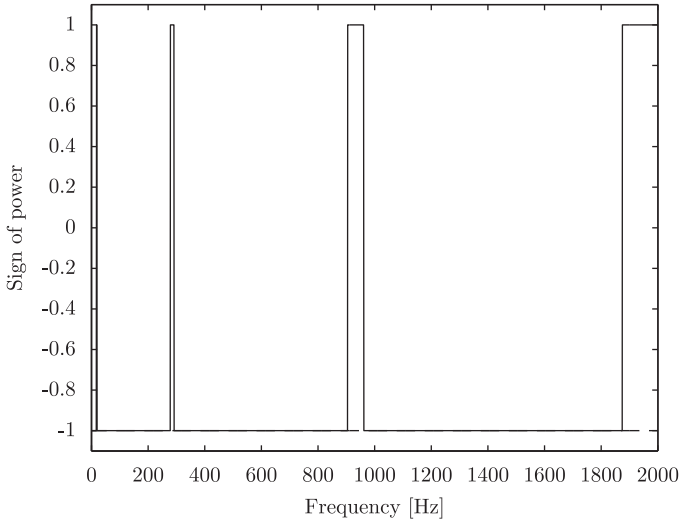

Fig. 12. The sign of the power injected or absorbed by the junction. A negative sign means that power was removed from the system while a positive sign means that power was inserted into the system. —: active impedance load; - - -: passive impedance.

8. Discussion

8.1. Maximum power transfer

A scalar impedance-matching technique (relating force and translational velocity) has been investigated with and without an incident near-field. The $(1,1)$ element of the reflection matrix becomes zero if the $(1,1)$ element of the active impedance matrix is chosen as half the complex conjugate of the corresponding characteristic impedance matrix, $(\tilde{Z}_{11}^{+})$. This agrees with previously reported results [1]. If only an incident wave is considered, the control law that cancels the reflected wave at a free end is equivalent to maximising the power absorbed by the active impedance load. Thus, this controller absorbs all incident power.

However, the controller performance diminishes if a significant near-field, together with the wave, is present at the junction. The incident near-field will reflect a propagating wave, which will carry power away from the

junction. This phenomenon is naturally most prominent at low frequencies where the near-field decay rate is low. If the primary force is located 1 m from the junction, the incident near-field becomes insignificant above 100 Hz; see Fig. 4. Thus, if the controller is designed to work above 100 Hz, the near-fields may in this case be neglected in the controller design. If the primary force is located 0.1 m from the junction, the near-field is significant in the entire investigated frequency range (1–2000 Hz); see Fig. 5. By using two elements in the active impedance matrix, relating translational and rotational velocities to force, the reflected wave can be avoided and all incident power is absorbed by the active impedance load (force). If the primary force is located 1 m from the junction, the interacting near-fields will contribute significantly to the net power flow below 100 Hz; see Fig. 6. If the primary force is located 0.1 m from the junction, the interacting near-fields propagate a significant amount of power in the entire investigated frequency range; see Fig. 7.

8.2. Active impedance matching between an Euler–Bernoulli beam and a sandwich composite

Fig. 9 shows that for the junction of the Euler–Bernoulli beam and the sandwich composite, a substantial part of an incident wave is reflected over a broad frequency band. Less than 1 dB of the incident wave is attenuated up to at least 2000 Hz. Thus, with only the PCLD most of the incident power is propagated back towards the primary excitation. However, the junction can be matched using impedance matching. If only a wave is incident at the junction, scalar impedance matching is sufficient to avoid the reflection of a propagating wave, i.e. element $(1,1)$ of the reflection matrix is set to zero.

Using impedance matching, all incident power is absorbed either by the active impedance load or in the PCL. Fig. 11 shows that the active impedance load absorbs most of the incident power while only a small part is dissipated in the sandwich composite. This holds for the entire investigated frequency range (1–2000 Hz), except around resonances where the active impedance load injects power. Fig. 10 shows that the control effort for matching the Euler–Bernoulli beam to the sandwich composite is generally greater than matching it to a free end. This makes sense as the free end is easier to move than the beam–sandwich composite junction.

The results indicate that an impedance-matching compensator which is driven to confine all incident wave power in a passive absorber works in theory, but does not offer significant advantages compared to previously investigated active control configurations. The impedance-matching compensator works virtually like a pure active absorber, off-resonance. However, using the passive–active configuration provides a fail-safe mechanism, i.e. the sandwich construction will always absorb some of the incident wave-field even in the absence of an active impedance load. For this configuration the active control works directly on the untreated beam, not through a viscoelastic layer as for an ACL. This is advantageous and the main reason for studies concerning improvement of the ACL, e.g. Refs. [28,29].

8.3. General conclusions

The impedance approach presented in this study has several advantages. First, it clearly shows how the reflection matrix at the interface between an Euler–Bernoulli and an arbitrary junction is affected by the impedance mismatch. It also allows a simple introduction of active control at this interface by adding an active impedance matrix to the passive impedance matrix. Control objectives can be specified by constraining the reflection matrix, and control laws can be derived analytically. Thus the concept of impedance matching is extended to the 2×2 impedance matrices used to describe an Euler–Bernoulli beam.

The impedance-matching problem for flexible structures has been treated in the past. However, this is the first time that impedance matching has been treated in full for the fourth-order Euler–Bernoulli PDE, hence also including the effect of an incident near-field. Results indicate that the scalar power transfer theorem has severe limitations in the presence of both incident wave and near-field.

The results from the study concerning using active control to enclose vibrational power in a sandwich composite suggest that the controller performs poorly around resonances where the active force injects power in the system. A way to cope with this problem may be to consider a more complex control law, e.g. including a penalty on control effort, thus reducing the resonance peaks for the control effort.

Acknowledgements

This work is funded by the Swedish research council, Project: 621-2004-5185.

Appendix A

A.1. Partial differential equation for the sandwich composite

The sandwich composite investigated in Section 7.2 is modelled using the equation derived in Ref. [26]. This model is based on Euler–Bernoulli theory for the base and cover beam, while only shear motion with a constant shear angle across the depth is assumed in the viscoelastic layer. This type of motion can be described by

$$\frac{\partial^6 \xi}{\partial x^6} - g(Y+1)\frac{\partial^4 \xi}{\partial x^4} + \frac{\rho}{D_t}\left(\frac{\partial^4 \xi}{\partial x^2 \partial t^2} - g\frac{\partial^2 \xi}{\partial t^2}\right) = 0, \tag{A.1}$$

where ξ represents the normal displacement of the structure, and ρ the density per unit length of the three-layer system. The quantities g, D_t and Y are given by

$$g = \frac{G}{t_v}\left(\frac{1}{E_b t_b} + \frac{1}{E_c t_c}\right), \tag{A.2}$$

$$D_t = E_b I_b + E_c I_c, \tag{A.3}$$

$$Y = b\frac{d^2}{D_t}\frac{E_b t_b E_c t_c}{E_b t_b + E_c t_c}, \tag{A.4}$$

where b, represents the width of the beam, and the subscripts b, c, and v denote base beam, cover beam and viscoelastic layer, respectively. G represents the complex shear modulus of the viscoelastic layer, defined by $G = G'(1 + j\eta)$, where G' is the storage modulus and η is the loss factor. The distance between the neutral lines of the base and cover layers is represented by d and is defined as

$$d = t_v + \frac{t_b + t_c}{2}. \tag{A.5}$$

A.2. Solution to the partial differential equation

Just as for Eq. (1), Eq. (A.1) can, by assuming harmonic motion, be solved with a wave approach. Inserting Eq. (2) into Eq. (A.1) yields a sixth-order polynomial whose roots represent the wavenumbers corresponding to wave types of this model. This yields the deflection field

$$\xi(x) = a_1 e^{\kappa_I x} + a_2 e^{-\kappa_I x} + a_3 e^{\kappa_{II} x} + a_4 e^{-\kappa_{II} x} + a_5 e^{\kappa_{III} x} + a_6 e^{-\kappa_{III} x}, \tag{A.6}$$

where $\kappa_I - \kappa_{III}$ are wavenumbers and $a_1 - a_6$ are unknown amplitudes which have to be adjusted according to boundary conditions and external excitation. The time dependence in Eq. (A.6) has been suppressed for simplicity. The wavenumbers, κ, are given by

$$\kappa_I^2 = \chi_1 + \chi_2 + \frac{g}{3}(Y+1), \tag{A.7}$$

$$\kappa_{II}^2 = -\frac{\chi_1 + \chi_2}{2} + j\frac{\sqrt{3}}{2}(\chi_1 - \chi_2) + \frac{g}{3}(Y+1), \tag{A.8}$$

$$\kappa_{III}^2 = -\frac{\chi_1 + \chi_2}{2} - j\frac{\sqrt{3}}{2}(\chi_1 - \chi_2) + \frac{g}{3}(Y+1), \tag{A.9}$$

where

$$\chi_1 = \sqrt[3]{-\frac{\zeta_2}{2} + \sqrt{\frac{\zeta_1^3}{27} + \frac{\zeta_2^2}{4}}}, \tag{A.10}$$

$$\chi_2 = \sqrt[3]{-\frac{\zeta_2}{2} - \sqrt{\frac{\zeta_1^3}{27} + \frac{\zeta_2^2}{4}}} \tag{A.11}$$

and

$$\zeta_1 = -\frac{\rho\omega^2}{D_t} - \frac{1}{3}g^2(Y+1)^2, \quad \zeta_2 = g\frac{\rho\omega^2}{D_t} - \frac{1}{3}g(Y+1)\frac{\rho\omega^2}{D_t} - \frac{2}{27}g^3(Y+1)^3. \tag{A.12}$$

A.3. Solving the unknown amplitudes

The six unknown amplitudes in Eq. (A.6) require six boundary conditions. In addition to the boundary conditions of the free–free Euler–Bernoulli beam that the bending moment and shear force are zero at the boundary, the longitudinal forces in the viscoelastic layer vanish at the boundaries. This gives in total six boundary conditions:

$$F(x=0) = 0, \quad F(x=L) = 0, \tag{A.13}$$

$$M(x=0) = 0, \quad M(x=L) = 0, \tag{A.14}$$

$$V(x=0) = 0, \quad V(x=L) = 0, \tag{A.15}$$

where V represents the longitudinal forces in the viscoelastic layer. The longitudinal force is given by

$$V = -\frac{D_t}{k_b bd}\left(\frac{1}{g}\frac{\partial^4\xi}{\partial x^4} - Y\frac{\partial\xi}{\partial x^2} - \frac{\rho\omega^2}{D_t g}\xi\right). \tag{A.16}$$

The bending moment is given by

$$M = \frac{D_t}{g}\left(\frac{\partial^4\xi}{\partial x^4} - (Y+1)g\frac{\partial^2\xi}{\partial x^2} - \frac{\rho\omega^2}{D_t}\xi\right), \tag{A.17}$$

and the shear force is given by

$$F = -\frac{D_t}{g}\left(\frac{\partial^5\xi}{\partial x^5} - g(Y+1)\frac{\partial^3\xi}{\partial x^3} - \frac{\rho\omega^2}{D_t}\frac{\partial\xi}{\partial x}\right). \tag{A.18}$$

References

[1] D. Guicking, J. Melcher, R. Wimmel, Active impedance control in mechanical structures, *Acustica* 69 (1989) 39–52.
[2] D. Pozar, *Microwave and RF Design of Wireless Systems*, Wiley, New York, 2001.
[3] A. Munshi, D. Johns, A. Sedra, Adaptive impedance matching, *IEEE International Symposium on Circuits and Systems*, Vol. 2, 1994, pp. 69–72.
[4] N.-T. Kim, Design of impedance-matching networks for microwave and millimeter-wave amplifier applications, *Microwave and Optical Technology Letters* 27 (2000) 109–113.
[5] L. Beranek, *Acoustics*, McGraw-Hill, New York, 1954.
[6] K. Nagase, H. Ojima, Y. Hayakawa, Wave-based analysis and wave control of ladder networks, *44th IEEE Conference on Decision and Control, and the European Control Conference*, 2005, pp. 5298–5303.
[7] J. Hu, J.-F. Lin, Active impedance control of linear one-dimensional wave equations, *International Journal of Control* 72 (1999) 247–257.

[8] S. Beyene, R. Burdisso, A new hybrid passive/active noise absorption system, *Journal of the Acoustical Society of America* 101 (1997) 1512–1515.
[9] J. Smith, B. Johnson, R. Burdisso, A broadband passive–active sound absorption system, *Journal of the Acoustical Society of America* 106 (1999) 2646–2652.
[10] J. Yuan, Causal impedance matching for broadband hybrid noise absorption, *Journal of the Acoustical Society of America* 113 (2003) 3226–3232.
[11] R. Glease, D. Miller, A generalized impedance matching method for determining structural-acoustic power flow control laws, *Journal of Sound and Vibration* 224 (1999) 283–303.
[12] R. Betros, O. Alvarez-Salazr, A. Bronowicki, Experiences with active damping and impedance matching compensators, *Proceedings of the SPIE—The International Society for Optical Engineering*, Vol. 1917, 1993, pp. 856–869.
[13] G. Kamath, P. Kumar, M. Shivaprasad, Vibration control using an impedance method, *Smart Materials, Structures and Systems* 5062 (2003) 509–516.
[14] A. Baz, Active constrained layer damping, *Damping 93 Conference*, Vol. 3, IBB, 1993, pp. 1–23.
[15] A. Baz, J. Ro, Partial treatment of flexible beams with active constrained layer damping, *Conference of Engineering Science Society*, Vol. ASME-AMD 67, Charlottesville, VA, 1993, pp. 61–80.
[16] H. Illare, A study of Active–Passive Damping Treatments, PhD Thesis, Chalmers University of Technology, 2004.
[17] M.J. Lam, D.J. Inman, W.R. Saunders, Vibration control through passive constrained layer damping and active control, *Journal of Intelligent Material Systems and Structures* 8 (1997) 663–677.
[18] Y. Liu, K.W. Wang, Damping optimization by integrating enhanced active constrained layer and active–passive hybrid constrained layer treatments, *Journal of Sound and Vibration* 255 (2002) 763–775.
[19] W.H. Liao, K.W. Wang, Characteristics of enhanced active constrained layer damping treatments with edge elements, part 1: finite element model development and validation, *Journal of Vibration and Acoustics* 120 (1998) 886–893.
[20] W.H. Liao, K.W. Wang, Characteristics of enhanced active constrained layer damping treatments with edge elements, part 2: system analysis, *Journal of Vibration and Acoustics* 120 (1998) 894–900.
[21] X. Pan, C. Hansen, Effect of end conditions on the active control of beam vibration, *Journal of Sound and Vibration* 168 (1992) 429–448.
[22] B. Mace, Wave reflection and transmission in beams, *Journal of Sound and Vibration* 97 (1984) 237–246.
[23] J. Svensson, P. Andersson, J. Scheuren, W. Kropp, Active scattering control of flexural waves at beam junctions: the influence of beam properties on power flow and control effort, *Journal of Sound and Vibration* 313 (2008) 418–432.
[24] J. Scheuren, Non-reflecting termination for bending waves in beams by active means, *Proceedings of the 1988 International Conference on Noise Control Engineering*, Noise Control Foundation, 1988, pp. 1065–1068.
[25] A. von Flotow, B. Schäfer, Wave-absorbing controllers for a flexible beam, *Journal of Guidance* 9 (1986) 673–680.
[26] D. Mead, S. Markus, The forced vibration of a three-layer, damped sandwich beam with arbitrary boundary conditions, *Journal of Sound and Vibration* 10 (1969) 163–175.
[27] H. Illare, W. Kropp, Quantification of damping mechanisms of active constrained layer treatments, *Journal of Sound and Vibration* 1–2 (2005) 189–217.
[28] M. Lam, D. Inman, W. Saunders, Variations of hybrid damping, *Proceedings of SPIE—The International Society for Optical Engineering*, Vol. 3327, 1998, pp. 32–43.
[29] W.H. Liao, K. Wang, A new active constrained layer configuration with enhanced boundary actions, *Smart Materials and Structures* 5 (1996) 638–648.